

# Ballooning stability of near-Earth plasma sheet during the March 23, 2007 THEMIS substorm event: A local analysis

P. Zhu,<sup>1</sup> J. Raeder,<sup>2</sup> K. Germaschewski,<sup>3</sup> A. Bhattacharjee,<sup>2</sup> and C. C. Hegna<sup>1</sup>

In this work, we analyze the ballooning properties of the near-Earth plasma sheet in the presence of magnetospheric convection, during the March 23, 2007 THEMIS substorm event. Using the solar wind data from WIND satellite observation for the substorm event as an input at dayside, we reconstructed a sequence of global magnetospheric configurations around the substorm onset by means of OpenGGCM simulation, which closely matches the observation in terms of onset timing. An approximate local dispersion relation for ballooning instability in the presence of flow is evaluated for the tail region when the configuration attains quasi steady-state conditions. Our analysis of the near-Earth tail region evolution during this substorm event starts to reveal the correlation between the breaching of the ballooning stability condition and the substorm onset, in both time and location. The analysis also indicates that the magnetospheric convection appears to have little direct effect on the ballooning instability itself; rather it plays a profound role by engaging the interaction between ballooning instability and reconnection in the plasma sheet.

Conventional scenarios of the substorm onset event invoke either current disruptions at the near-Earth magnetotail or magnetic reconnection processes in the middle magnetotail. Both scenarios have been built on suggestive but sometimes ambiguous observational and theoretical evidence (See, for example, [Lui, 2003]). The ambiguity results in part from the lack of sufficient resolution in data, in both observations and simulations. On the other hand, it appears that the trigger mechanism may actually involve multiple entangled processes [Voronkov *et al.*, 2004]. In this work, we suggest a particular multi-step process for the substorm onset, where ballooning instabilities can be induced by reconnection and convection that steepen the pressure gradient.

Most previous investigations of ballooning instabilities in the near-Earth magnetotail have been carried out under the assumption of a magnetostatic magnetosphere that is absent of either convection or reconnection [Miura *et al.*, 1989; Hameiri *et al.*, 1991; Lee and Wolf, 1992; Pu *et al.*, 1992; Ohtani and Tamao, 1993; Hurricane *et al.*, 1995, 1996, 1997; Pu *et al.*, 1997; Bhattacharjee *et al.*, 1998; Cheng and Lui, 1998; Lee, 1999; Wong *et al.*, 2001; Crabtree *et al.*, 2003; Zhu *et al.*, 2003; Cheng and Zaharia, 2004; Schindler and Birn, 2004; Zhu *et al.*, 2004, 2007]. In reality, the magnetosphere exhibits persistent convection and reconnection in

the tail region, which is often intermittent, as evidenced by the presence of bursty bulk flows in both observations and simulations. The three major processes, ballooning, reconnection, and convection, each may have contributed indispensably to the onset of a substorm. The roles of each, and the interactions among them, may hold a key to understanding the trigger mechanism of substorm onset.

Recent observations from the multi-satellite mission THEMIS and global MHD simulations of the March 23, 2007 substorm event (hereafter referred to as THEMIS substorm event) provide a unique opportunity for us to examine more closely the roles of ballooning instability and magnetic reconnection in the presence of magnetospheric convection in the triggering of a substorm onset. Using WIND solar wind data for the THEMIS substorm event, a sequence of global magnetospheric configurations have been reconstructed around the substorm onset by means of OpenGGCM simulations [Raeder, 2003; Raeder *et al.*, 2007]. Our local ballooning analysis of the near-Earth magnetotail configurations revolving around the onset event starts to reveal the role of magnetospheric convection, the interaction between ballooning instability and reconnection, and the correlation between the breaching of the ballooning stability boundary and the substorm onset. In rest of this letter we briefly report the analysis and findings.

The OpenGGCM simulation in this study covers a spatial domain of  $x : [20, -500]$ ,  $y : [-36, 36]$ ,  $z : [-36, 36]$  where GSM coordinates are used and one unit of length is the Earth radius ( $R_E$ ). The size of the nonuniform Cartesian grid is  $315 \times 100 \times 150$ , with  $(\Delta x)_{\min} = 0.29$ ,  $(\Delta y)_{\min} = 0.25$ ,  $(\Delta z)_{\min} = 0.16$ , where  $(\Delta x)_{\min}$ ,  $(\Delta y)_{\min}$ ,  $(\Delta z)_{\min}$  are the minimum grid spacings in three coordinate directions, respectively. In order to reconstruct the THEMIS March 23, 2007 substorm event, the solar wind data from satellite WIND near the dayside magnetopause is used to impose the dayside boundary conditions. The ionosphere boundary conditions are determined by the Coupled Thermosphere Ionosphere Model (CTIM) [Fuller-Rowell *et al.*, 1996]. Shown in Fig. 1 is the pressure isosurface in the entire spatial domain in actual scale, together with pressure contours in equatorial and meridional planes at the UT 10:00 from simulation.

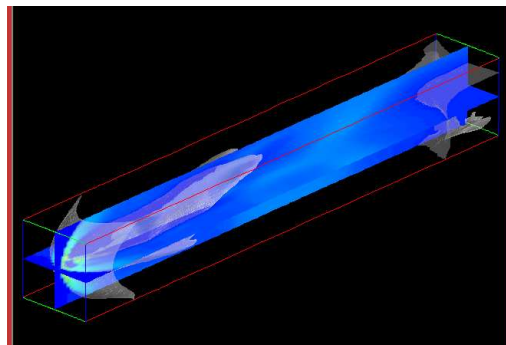


**Figure 1.** Pressure isosurface and pressure contours in equatorial and meridional planes at UT 10:00 from the simulation. The bounding box encloses the entire spatial domain of simulation.

<sup>1</sup>Center for Plasma Theory and Computation, University of Wisconsin-Madison, Madison, WI 53706

<sup>2</sup>Space Science Center and Center for Magnetic Self Organization, University of New Hampshire, Durham, NH 03824

<sup>3</sup>Department of Computer Science, College of Staten Island, City University of New York, Staten Island, NY 10314

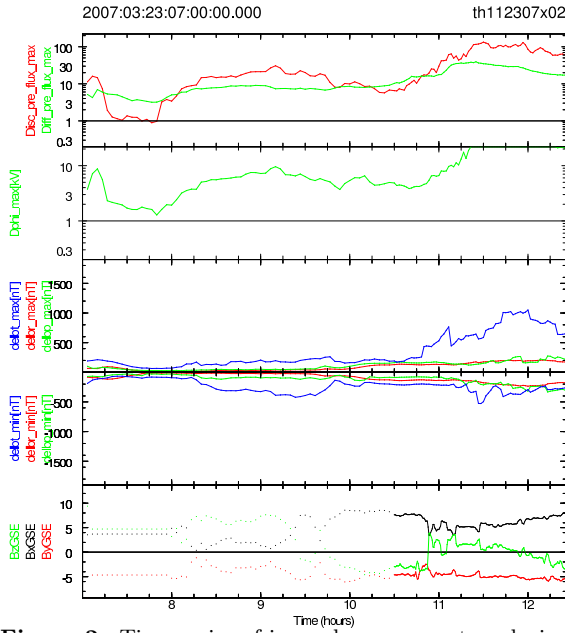


**Figure 2.** Time series of ionosphere parameters during UT 08:00~12:00 from simulation: Discrete and diffuse auroral electron precipitation energy flux [ $\text{mW}/\text{m}^2$ ] (first panel); maximum Knight potential (second panel); maximum (third panel) and minimum (fourth panel) ground magnetic perturbations; magnetic field at upper stream location (16,0,0) of bow shock (fifth panel).

The time series of the discrete auroral electron precipitation energy flux from simulation indicates that the aurora brightening starts around UT 10:45, consistent with the substorm onset timing also suggested by the time series of Knight potential and ground magnetic perturbation (Fig. 2). The timing of the simulated substorm onset closely matches the THEMIS ground and in-situ observations of the event [Raeder *et al.*, 2007]. The northward turning of the magnetic field upstream of the bow shock occurs slightly later than the onset time (Fig. 2). We now take a close look at four representative snapshots of the near-Earth magnetotail configurations around the substorm onset. In particular we focus on the series of pressure and tailward flow patterns within the domain  $x : [-5, -40]$ ,  $z : [-5, 5]$  in the meridional plane (Fig. 3).

- UT 10:00: The ionosphere and ground magnetic activity levels are low, and the near-Earth region ( $-x \sim 5 - 20 R_E$ ) of the plasma sheet is wide and moderately stretched, as seen from the pressure pattern. At the same time, the tailward flow pattern indicates that reconnection is taking place around  $x = -31 R_E$  down in the middle magnetotail. The mid-tail reconnection produces a maximum Earthward flow of about 400 km/s.

- UT 10:43: As indicated from the ionosphere and ground magnetic perturbation time series in Fig. 2, substorm onset starts to initiate. The pressure pattern at that time shows a substantial thinning and stretching of the near-Earth magnetotail. In the meantime, the reconnection site has moved Earthward to around  $x = -10 R_E$ , where the plasma sheet thinning occurs most. The maximum Earthward flow at this

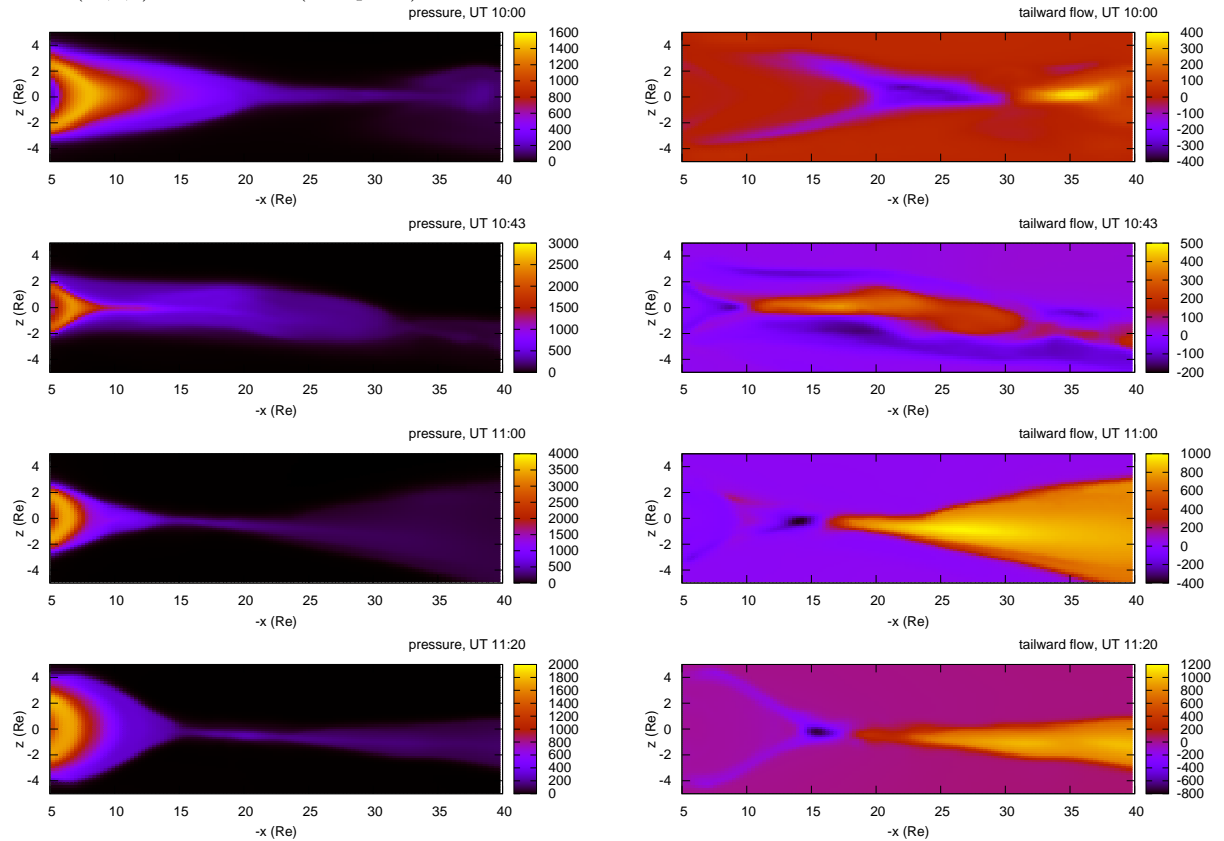


**Figure 3.** Pressure (left column) and tailward flow (right column) patterns in meridional plane at four time slices.

reconnection site has now reduced to about 100 km/s, due to the increase of pressure as well as the steepening of the Earthward pressure gradient. The maximum tailward flow out of the reconnection is about 500 km/s.

- UT 11:00: A full onset is in progress. In the near-Earth region the pressure and its Earthward gradient continue to build up to their maximums during the time series, whereas the tailward flow due to the reconnection around  $x = -10 R_E$  also almost doubled its magnitude ( $\sim 1000$  km/s), indicating an enhanced level of reconnection. The reconnection site has receded tailward to  $x = -16 R_E$ , and the previously stretched and thin plasma sheet in the near-Earth region ( $-x \lesssim 10 R_E$ ) starts to dipolarize.

- UT 11:20: When the event enters the expansion phase, the pressure and its gradient in the near-Earth region start to decrease. The magnetotail configuration in that region ( $-x \lesssim 10 R_E$ ) becomes further dipolarized. The tailward flow from the reconnection site, which shifts slightly further tailward to about  $x = -17 R_E$ , remains at the same high level as earlier at UT 11:00.

The above time series of pressure and tailward flow patterns clearly show the correlation between the plasma sheet intensification and relaxation and the convection of the reconnection site. Next we will look into how the ballooning properties of the near-Earth plasma sheet evolve in that time series.

For a magnetotail configuration in the presence of convection along the Sun-Earth ( $x$ ) direction, its equilibrium can be described by  $\nabla(p + \rho u_x^2/2) = \mathbf{J} \times \mathbf{B}$ , and correspondingly

the growth of its ballooning instability may be estimated using the following relation

$$\Gamma_{\text{bal}}^2 \simeq -\Gamma_{\text{ben}}^2 + \Gamma_{\text{int}}^2 - \Gamma_{\text{con}}^2 \quad (1)$$

where

$$\Gamma_{\text{bal}}^2 \xi = \frac{\partial^2 \xi}{\partial t^2} \quad (2)$$

$$\Gamma_{\text{ben}}^2 \xi = -\frac{B^3}{\rho} \frac{\partial}{\partial l} \left( \frac{1}{B} \frac{\partial \xi}{\partial l} \right) \lesssim \left( \frac{u_A}{R_E} \right)^2 \xi = \frac{B^2 \xi}{\rho R_E^2} \quad (3)$$

$$\Gamma_{\text{int}}^2 \xi = \frac{2B\kappa_\Psi}{\rho} \frac{dp}{d\Psi} \xi \quad (4)$$

$$\Gamma_{\text{con}}^2 \xi \simeq \left( \frac{u_x}{L_p} \right)^2 \xi \quad (5)$$

and  $L_p^{-1} = |d \ln p / dx|$ . Here  $\Gamma_{\text{bal}}$  is the ballooning growth rate,  $\Psi$  the magnetic flux function defining the configuration,  $\xi$  the plasma displacement across the flux surface,  $\kappa_\Psi$  the normal component of magnetic curvature,  $\rho$  the mass density,  $p$  the pressure,  $u_x$  the tailward flow velocity,  $u_A$  the Alfvén speed,  $B$  the magnitude of magnetic field, and  $l$  the field line length. The line bending parameter  $\Gamma_{\text{ben}}$ , interchange parameter  $\Gamma_{\text{int}}$ , and the convection parameter  $\Gamma_{\text{con}}$  represent the inverse of the time scales associated with shear-Alfvén wave, interchange force, and convection, respectively. Ballooning instability requires  $\Gamma_{\text{int}}^2 > \Gamma_{\text{con}}^2$  and

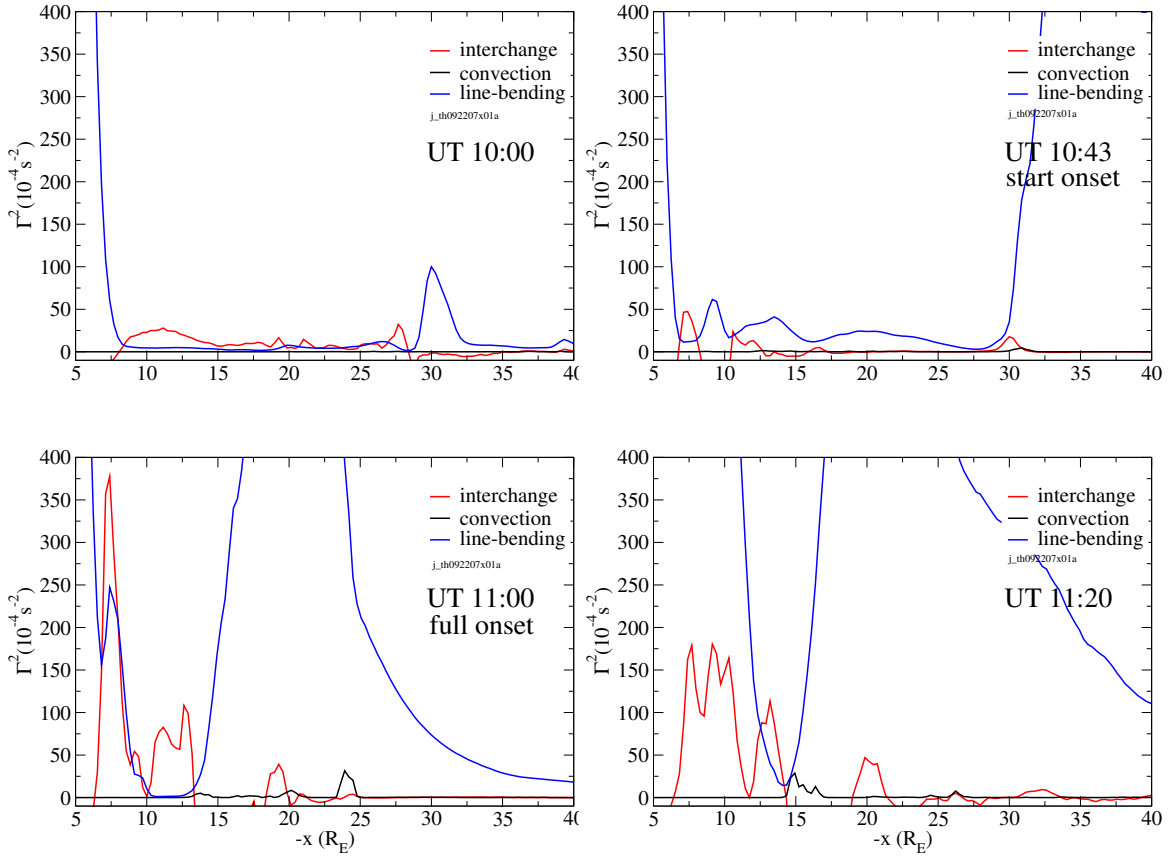


**Figure 4.** Interchange drive  $\Gamma_{\text{int}}^2$ , line bending force  $\Gamma_{\text{ben}}^2$ , and convection contribution  $\Gamma_{\text{con}}^2$  along line  $y = z = 0$  in the near-Earth tail region at four representative times.

$\Gamma_{\text{int}}^2 > \Gamma_{\text{ben}}^2$ . The relation in (1) is basically an approximate local dispersion relation for a ballooning mode of the magnetotail in presence of convection across flux surfaces. In the local approximation and near marginal stability, the influence of ionosphere boundary and the plasma compression may be ignored. A rigorous derivation of the relation in (1), and the nonlocal eigenvalue analysis for the ballooning mode will be reported in forthcoming papers.

We examine the overall ballooning properties of the near-Earth plasma sheet during the substorm onset by evaluating the criterion (1) for the magnetotail configurations at the same four representative time slices, as described in earlier section. As the first step, the interchange parameter  $\Gamma_{\text{int}}^2$ , the line bending parameter  $\Gamma_{\text{ben}}^2$ , and the convection parameter  $\Gamma_{\text{con}}^2$  are evaluated along the  $y = 0, z = 0$  line in equatorial and meridional planes, for each time slice. The results are shown in Fig. 4 and summarized below.

- UT 10:00: At this stage, most of the near-Earth tail region between  $x = -7.5 R_E$  and  $x = -30 R_E$  is marginally unstable. For  $-x \lesssim 7.5 R_E$  and  $-x \gtrsim 30 R_E$ , the line bending force  $\Gamma_{\text{ben}}^2$  is dominant, whereas in between ( $-x \sim 7.5 - 30 R_E$ ), the line bending force  $\Gamma_{\text{ben}}^2$  significantly drops, forming a “well” shaped profile for  $\Gamma_{\text{ben}}^2$ . Within this well shaped region, the magnitude of  $\Gamma_{\text{ben}}^2$  is comparable to and slightly smaller than that of the interchange force  $\Gamma_{\text{int}}^2$ , resulting in a marginally unstable state. The contribution from convection directly to ballooning growth, as estimated by  $\Gamma_{\text{con}}^2$ , is rather small in the entire tail region considered.

- UT 10:43: Around this time when the onset initiates, the shape of the well in the field line bending force appears largely unchanged. The overall balance between  $\Gamma_{\text{ben}}^2$  and  $\Gamma_{\text{int}}^2$  is similar to the previous time stage, and the near-Earth tail region remains marginally stable.

- UT 11:00: The ballooning properties of the near-Earth tail region dramatically change during this full onset phase. The width of the well in the field line bending force significantly shrinks from  $22.5 R_E$  at UT 11:00 to about  $7.5 R_E$ , and the center (bottom) of the well shifted from  $17.5 R_E$  to around  $10 R_E$ , due mostly to the Earthward shift of the tail-side boundary of the well. Within the well, the interchange drive  $\Gamma_{\text{int}}^2$  rises to peak values ( $\sim 0.01 - 0.0375$ ) that are 2 to 7 times larger than previous time slices ( $\sim 0.005$ ). Since the direct contribution from convection  $\Gamma_{\text{con}}^2$  remains negligibly low, the surge of the interchange drive  $\Gamma_{\text{int}}^2$  in the localized well between  $6 R_E$  and  $14 R_E$ , makes this narrow region in the near-Earth tail ballooning unstable.

- UT 11:20: In this phase, the well in the field line bending force has shrunk to a very narrow region around  $14 R_E$ , within which the line bending force  $\Gamma_{\text{int}}^2$  and the interchange drive  $\Gamma_{\text{int}}^2$  becomes comparable again. As a result, the near-Earth tail region becomes stable or marginally stable to ballooning instability.

The above development of ballooning properties shows a close correlation between the breaching of local ballooning instability criterion and the full onset of the substorm event in both time and location. Over the entire near-Earth tail region and its progression, the tailward and Earthward convections do not seem to directly affect ballooning instability itself.

However, the Earthward convection in magnetotail appears to play a rather profound role leading to the substorm onset, by connecting and coupling the middle tail reconnection and the near-Earth tail ballooning processes. Our simulation and analysis indicate that it is the Earthward convection of the tail reconnection site that leads to the build-up of the pressure gradient and the surge of interchange drive, as well as a weakening of line-bending force in

the near-Earth region ( $-x \sim 6 - 14 R_E$ ). Note that there is a short time delay of 17 minutes between the arrival of the reconnection site at about  $x = -10 R_E$  at UT 10:43 (Fig. 3) and the surge in interchange drive and ballooning growth in the  $6 - 14 R_E$  region at UT 11:00 (Fig. 4). It is conceivable that the Earthward convection of the reconnection site as well as the Earthward flow from reconnection itself has preconditioned the near-Earth tail region for the rise of ballooning instability in a narrow temporal and spatial window that coincides and may actually lead to the full onset of the substorm event. The greatly enhanced reconnection as indicated by the increased level of tailward flow from reconnection site at and after the full onset (UT 11:00) could be one outcome of the sudden rise of ballooning instability in the  $6 - 14 R_E$  region. It is worth noting that the observations here on the interaction among convection, reconnection, and ballooning instability leading to the onset of substorm is consistent with the similar findings from an earlier ballooning analysis of the magnetospheric configurations obtained from a 2D Hall MHD simulation of the substorm onset process [Zhu et al., 2003; Ma and Bhattacharjee, 1998].

In summary, the local marginal ballooning criterion that crudely takes into account the effects of convection is applied to the analysis of the near-Earth magnetotail configurations obtained from OpenGGCM simulations for the THEMIS substorm event on March 23, 2007. Simulation and analysis indicate that the full onset event is closely correlated to the breaching of ballooning criterion in both time and location. The Earthward convection in the magnetotail does not directly affect ballooning instability itself; rather, the Earthward convection of the reconnection site appears to help set up a favorable condition for the onset of a robust ballooning instability by building up the pressure gradient and weakening the line-bending force in the near-Earth tail region.

The local ballooning analysis in this letter is a first step aimed at identifying the roles of convection, ballooning, and reconnection in a substorm onset process, to lowest and dominant order. Global ballooning analysis by solving the eigenmode equations along each flux tube under exact boundary conditions will be reported in subsequent publications.

**Acknowledgments.** This research is supported by NSF Grant No. ATM-0542954. Computations were performed in NERSC, which is supported by DOE under Contract No. DE-AC03-76SF00098, on the Zaphod Beowulf cluster which was in part funded by the MRI program of the NSF under grant ATM-0420905, and through NSF TeraGrid resources provided by SDSC. P. Zhu is grateful for discussions with Prof. F. Toffoletto.

## References

- Bhattacharjee, A., Z. W. Ma, and X. Wang, Ballooning instability of a thin current sheet in the high-lundquist-number magnetotail, *Geophys. Rev. Lett.*, *25*, 861–864, 1998.
- Cheng, C. Z., and A. T. Y. Lui, Kinetic ballooning instability for substorm onset and current disruption observed by AMPTE/CCE, *Geophys. Rev. Lett.*, *25*, 4091–4094, 1998.
- Cheng, C. Z., and S. Zaharia, MHD ballooning instability in the plasma sheet, *Geophys. Rev. Lett.*, *31*, L06,809, doi: 10.1029/2003GL018823, 2004.
- Crabtree, C., W. Horton, H. V. Wong, and J. W. V. Dam, Bounce-averaged stability of compressional modes in geotail flux tubes, *J. Geophys. Res.*, *108*, 1084, doi: 10.1029/2002JA009555, 2003.
- Fuller-Rowell, T. J., D. Rees, S. Quegan, R. J. Moffett, M. V. Codrescu, and G. H. Millward, A coupled thermosphere-ionosphere model (CTIM), in *STEP Report*, edited by R. W. Schunk, p. 217, Scientific Committee on Solar Terrestrial Physics (SCOSTEP), NOAA/NGDC, Boulder, Colorado, 1996.

- Hameiri, E., P. Laurence, and M. Mond, The ballooning instability in space plasmas, *J. Geophys. Res.*, *96*, 1513–1526, 1991.
- Hurricane, O. A., R. Pellat, and F. V. Coroniti, The stability of a stochastic plasma with respect to low frequency perturbations, *Phys. Plasmas*, *2*, 289–293, 1995.
- Hurricane, O. A., R. Pellat, and F. V. Coroniti, Instability of the Lembège-Pellat equilibrium under ideal magnetohydrodynamics, *Phys. Plasmas*, *3*, 2472–2474, 1996.
- Hurricane, O. A., B. H. Fong, and S. C. Cowley, Nonlinear magnetohydrodynamic detonation: Part I, *Phys. Plasmas*, *4*, 3565, 1997.
- Lee, D.-Y., Stability analysis of the plasma sheet using Hall magnetohydrodynamics, *J. Geophys. Res.*, *104*, 19,993–19,999, 1999.
- Lee, D.-Y., and R. A. Wolf, Is the earth's magnetotail balloon unstable?, *J. Geophys. Res.*, *97*, 19,251–19,257, 1992.
- Lui, A. T. Y., Cause of magnetospheric substorms, *Plasma Phys. Control. Fusion*, *45*, 841–852, 2003.
- Ma, Z. W., and A. Bhattacharjee, Sudden enhancement and partial disruption of thin current sheets in the magnetotail due to Hall MHD effects, *Geophys. Res. Lett.*, *25*, 3277–3280, 1998.
- Miura, A., S. Ohtani, and T. Tamao, Ballooning instability and structure of diamagnetic hydromagnetic waves in a model magnetosphere, *J. Geophys. Res.*, *94*, 15,231–15,242, 1989.
- Ohtani, S., and T. Tamao, Does the ballooning instability trigger substorms in the near-Earth magnetotail?, *J. Geophys. Res.*, *98*, 19,369, 1993.
- Pu, Z. Y., A. Korth, and G. Kremser, Plasma and magnetic field parameters at substorm onsets derived from GEOS 2 observations, *J. Geophys. Res.*, *97*, 19,341, 1992.
- Pu, Z. Y., A. Korth, Z. X. Chen, R. H. W. Friedel, Q. G. Zong, X. M. Wang, M. H. Hong, S. Y. Fu, Z. X. Liu, and T. I. Pulkkinen, MHD drift ballooning instability near the inner edge of the near-earth plasma sheet and its application to substorm onset, *J. Geophys. Res.*, *102*, 14,397–14,406, 1997.
- Raeder, J., Global Geospace Modeling: Tutorial and Review, in *Space Plasma Simulation*, edited by J. Büchner, C. T. Dum, and M. Scholer, Springer Verlag, Berlin Heidelberg New York, 2003.
- Raeder, J., L. Kepko, E. Kaghshvili, V. Angelopoulos, D. Larson, J. McFadden, C. Carlson, K. Glassmeier, U. Auster, and G. Parks, OpenGGCM simulation of the March 23, 2007 substorm observed by THEMIS, in *Eos Trans. AGU, Fall Meet. Suppl.*, vol. 88 (52), American Geophysical Union, abstract SM21C-08, 2007.
- Schindler, K., and J. Birn, Mhd stability of magnetotail equilibria including a background pressure, *J. Geophys. Res.*, *109*, A10,208, doi:10.1029/2004JA010537, 2004.
- Voronkov, I. O., E. F. Donovan, P. Dobias, V. I. Prosofin, M. Jankowska, and J. C. Samson, Late growth phase and breakup in the near-earth plasma sheet, in *Proceedings of the 7th International Conference on Substorms (ICS-7), Levi, Finland, 2004*, p. 140, 2004.
- Wong, H. V., W. Horton, J. W. Van Dam, and C. Crabtree, Low frequency stability of geotail plasma, *Phys. Plasmas*, *8*, 2415–2424, 2001.
- Zhu, P., A. Bhattacharjee, and Z. W. Ma, Hall magnetohydrodynamic ballooning instability in the magnetotail, *Phys. Plasmas*, *10*, 249–258, 2003.
- Zhu, P., A. Bhattacharjee, and Z. W. Ma, Finite- $k_y$  ballooning instability in the near-Earth magnetotail, *J. Geophys. Res.*, *109*, A11,211, doi:10.1029/2004JA010505, 2004.
- Zhu, P., C. R. Sovinec, C. C. Hegna, A. Bhattacharjee, and K. Germaschewski, Nonlinear ballooning instability in the near-Earth magnetotail: Growth, structure, and possible role in substorms, *J. Geophys. Res.*, *112*, A06,222, doi:10.1029/2006JA011991, 2007.

---

C. C. Hegna and P. Zhu, 1500 Engineering Drive, Madison, WI 53706 (heгна@cae.wisc.edu; pzhou@wisc.edu); A. Bhattacharjee and J. Raeder, 39 College Road, Durham, NH 03824 (amitava.bhattacharjee@unh.edu; j.raeder@unh.edu); K. Germaschewski, 2800 Victory Boulevard, Staten Island, NY 10314 (germaschewski@mail.csi.cuny.edu).